Published in final edited form as:
Proteins. 2010 February 1; 78(2): 434–446. doi:10.1002/prot.22560.

RNA Polymerase II Flexibility During Translocation From Normal Mode Analysis

Michael Feig[1,2,*] and **Zachary F. Burton**[1]

[1]Department of Biochemistry and Molecular Biology, Michigan State University, East Lansing, MI 48824; USA

[2]Department of Chemistry, Michigan State University, East Lansing, MI 48824; USA

Abstract

The structural dynamics in eukaryotic RNA polymerase II (RNAPII) is described from computational normal mode analysis based on a series of crystal structures of pre- and post-translocated states with open and closed trigger loops. Conserved modes are identified that involve translocation of the nucleic acid complex coupled to motions of the enzyme, in particular in the clamp and jaw domains of RNAPII. A combination of these modes is hypothesized to be involved during active transcription. The NMA modes indicate furthermore that downstream DNA translocation may occur separately from DNA:RNA hybrid translocation. A comparison of the modes between different states of RNAPII suggests that productive translocation requires an open trigger loop and is inhibited by the presence of an NTP in the active site. This conclusion is also supported by a comparison of the overall flexibility in terms of root mean square fluctuations.

Keywords

transcription; translocation; nucleic acids; root mean square fluctuations; mode robustness

Introduction

Transcription – the synthesis of RNA based on DNA – is an exceedingly complex and highly regulated process that is accomplished at the core by RNA polymerases. Bacterial RNA polymerase consists of five subunits with a sixth subunit involved only during the initiation of transcription. Eukaryotic RNA polymerases have many more subunits – RNA polymerase II has 12 subunits – and they involve a large number of additional transcription and other accessory factors in order to implement more precise regulatory mechanisms, couple to chromatin remodeling, and effectuate a higher degree of transcriptional fidelity[1–3]. Much insight into RNA polymerase function has resulted from a series of crystal structures of bacterial RNA polymerases and eukaryotic RNA polymerase II from *S. cerevisiae* (referred to as RNAPII)[4,5]. Both enzymes exhibit a similar architecture with a large DNA binding cleft that is flanked by the clamp and jaw domains and an active site that is partially buried at the center of the enzyme. While many previous studies, especially computational studies, have focused on bacterial RNA polymerase because of its relative simplicity this study describes RNAPII.

Characteristic features of RNAPII include the bridge helix (rpb1 811–845), the trigger loop/helix (rpb1 1075–1100), and the fork loop 2 (rpb2 500–510) that are conserved among both enzymes. Available crystal structures of RNAPII cluster into conformations with open and

*Corresponding author: Phone: (517) 432-7439, FAX: (517) 353-9334, feig@msu.edu.

closed clamp domains, where open forms are only seen in the absence of nucleic acid[6]. At the same time, electron microscopy[7] and FRET microscopy[8] studies of bacterial RNA polymerase suggest that the RNA polymerase structure may exhibit significant conformational flexibility. However, little detailed information is available to date about the dynamic properties of RNA polymerase how they relate to its function.

An unresolved key question is how DNA/RNA translocation is accomplished mechanistically. Translocation advances the nucleic acid complex after addition of a new nucleotide to the nascent RNA strand in order to begin the next nucleotide incorporation cycle. Two different models have been proposed to explain the translocation process: In the more widely accepted passive Brownian ratchet mechanism, the DNA:RNA hybrid stochastically rattles between pre- and post-translocated states as a result of thermal fluctuations, where the binding of a nucleotide to the active site would lock the enzyme into the post-translocated state[9–14]. A variation of this model is the idea of NTP-driven translocation where correctly templated pre-bound nucleotides would favor a transition to the post-translocated state[15]. In the Brownian ratchet model the mechanism of coupling translocation and nucleotide incorporation is not clear and hyper-translocation by two or more base pairs may be possible, as demonstrated in T7 RNA polymerase[16]. In the alternative power stroke model it is assumed that the enzyme plays a more active role by utilizing the energy released during nucleotide incorporation to drive forward the transition from the pre- to the post-translocated state[17]. In both cases, RNA polymerase is expected to undergo significant transient conformational changes. Specifically, bending of the bridge helix during translocation has been proposed previously[9]. One goal of the present study is to determine the extent and role of bridge helix bending during translocation. Another goal is to examine to what extent other parts of the enzyme, for instance the trigger loop/helix, may be involved during translocation. The transition from a partially disordered trigger loop conformation to an ordered helical conformation has been suggested as the key step in authorizing the incorporation of a correctly templated nucleotide residing in the active site[18,19]. It is not clear, however, whether translocation requires an open or closed trigger loop conformation.

Previous studies of RNA polymerase flexibility and dynamics include molecular dynamics simulations of the single subunit T7 RNA polymerase system where the transition between pre- and post-translocated states of the DNA:RNA hybrid have been reported recently[20]. Furthermore, normal mode analyses of bacterial and T7 RNA polymerase have described the overall enzyme flexibility with a focus on the jaw opening motion[21–23]. Neither study describes the dynamics of RNA polymerase during translocation. Furthermore, neither study addresses the dynamics and flexibility of the eukaryotic enzyme RNAPII.

Here, normal mode calculations of RNAPII based on recent new crystal structures are presented to identify possible enzyme motions related to translocation. The specific hypothesis tested here is that translocation is in fact coupled to bridge helix bending and that translocation requires an open trigger loop state. In order to address this specific question and explore RNAPII flexibility more generally, NMA results of pre- and post-translocated RNAPII with open and closed trigger loops are compared. These structures represent the major states during RNAPII's functional cycle. The cycle begins with the post-translocated open trigger loop form (RNAPII-open, see Table 1) with an empty active site, followed by the open trigger loop NTP-bound form (RNAPII-ntp). Trigger loop dynamics then leads to the closed trigger loop NTP-bound form (RNAPII-closed) and finally the pre-translocated state with an open trigger loop (RNAPII-pre) is reached.

Normal mode analysis (NMA) results in a decomposition of structural fluctuations around a structure at a local minimum into modes based on a harmonic approximation of the

underlying molecular interaction potential. Often highly simplified interaction potentials such as elastic network models are used in NMA calculations. Here, we employ a fully atomistic force field to describe intramolecular interactions. Such a potential is more expensive but includes a full account of electrostatic and dispersion interactions and has been shown to yield qualitatively improved results[24].

The complete mode spectrum contains information about the flexibility of different parts of the structure, while the lowest-frequency modes that involve global deformations of the entire structure often correspond to biologically relevant motions in biological macromolecules. Normal mode calculations also have limitations that should be considered. NMA-derived modes are strictly valid only for a single structure and do not provide direct information about other states that may be visited during dynamics. However, NMA-derived modes often indicate a likely direction of transitions to other states in an idealized fashion from which hypotheses about actual conformational dynamics may be deduced. Furthermore, a more complete picture of the dynamics of a given system may be obtained by carrying out NMA for a number of different structures, as in this study.

Other potential problems with normal mode calculations are a lack of robustness of the resulting modes and the occurrence of mixing between multiple modes that complicate their interpretation. We have addressed this issue by comparing modes from different structures of RNAPII and found that mixing between the ten lowest-frequency modes appears to be limited.

Another limitation is that a focus on low-frequency modes ignores a possibly important role of local conformational changes during translocation. The current study will not be able to address such cases and remains focused on global changes in RNAPII during translocation.

Despite limitations of NMA, normal mode calculations are attractive because they allow the study of dynamic motions in very large molecules, which otherwise are extremely challenging in computational studies. Furthermore, while we suggest that new insight about the dynamics of the translocation mechanism in RNAPII has been gained from the present study, the results should be viewed predominantly as a means to generate more specific new hypotheses that can be tested in subsequent experiments or computational studies.

The computational methodology is described in more detail next, followed by the presentation and discussion of the results.

Methods

Starting structures

NMA calculations were carried out for four recent 10-subunit RNAPII structures as summarized in Table 1. This study emphasizes the comparison of structures with trigger loop (open) and trigger helix (closed) conformations. Furthermore, open trigger loop structures were analyzed in pre-insertion (RNAPII-ntp), pre-translocation (RNAPII-pre), and post-translocation (RNAPII-open) forms. The structures deposited in the PDB were used as is, including all metal ions. Missing residues in the open trigger loop (rpb1 1082–1091) and in fork loop 2 (rpb2 503–508) were completed through loop modeling using Modeller[25,26]. Other missing residues in rpb1, rpb2, and rpb8 corresponding to surface loops were not completed because they are unlikely to affect the global lowest-frequency modes. The post-translocation structure was obtained by simply omitting the GTP from the crystal structure (2E2J). The pre-translocation structure was constructed by removing the secondary and tertiary phosphates from the active site GTP (at the i+1 site) and introduction of a covalent bond between the monophosphate and the first (i) RNA base. The resulting

structure was relaxed during brief energy minimization during 50 cycles of steepest descent minimization followed by 1000 cycles of adopted-basis Newton-Raphson minimization with CHARMM[27] using the CHARMM22 force field[28] and distance dependent dielectric and additional restraints to keep the newly incorporated nucleotide in place.

Normal mode analysis

Normal mode analysis (NMA)[29] involves diagonalization of the Hessian matrix H with the elements:

$$H_{ij}=\frac{\partial^2 V}{\partial q_i \partial q_j} \quad (1)$$

where V(q) is a given intramolecular interaction potential. The result is a set of eigenvectors and eigenvalues that correspond to normal modes and associated frequencies, respectively. For a given biomolecular system, the lowest-frequency modes are often biologically relevant because they describe motions that encompass the entire system and provide information about dynamic coupling between distant sites[30–33]. The diagonalization of the Hessian matrix as given in Eq. 1 becomes computationally intractable for large biomolecules such as RNA polymerase if a fully atomistic model and force field is applied. This problem can be overcome through the use of a simplified interaction potential based on coarse-grained interaction sites that are connected by harmonic springs as is done in the widely used elastic network models (ENM)[34]. An alternative is the block-normal mode (BNM) approach that maintains a fully atomistic model and interaction potential but projects the full Hessian onto a subspace where each residue moves as a rigid block so that sparse matrix diagonalization techniques can be applied[35,36]. The mode spectrum from BNM analysis is essentially identical to conventional NMA for the lowest frequency modes but differs significantly for higher frequency modes where intra-residue motions become important[24,35].

Here, the BNM approach was chosen so that the more accurate energetic description according to an atomistic force field could be used. The BNM implementation within the VIBRAN module of CHARMM[37], version c34a2, was used in conjunction with the CHARMM27 all-atom force field for proteins and nucleic acids[28,38] including CMAP backbone torsion terms[39]. Parameters for nucleotides were constructed by combining parameters for ATP with other bases from the nucleic acid force field[38]. Altered charges were used for Zn^{2+}-bound cysteines (C_β: −0.35, $H_{\beta1}/H_{\beta2}$: 0.05, S_γ: −0.75) to reflect deprotonation in the presence of the metal. The effect of solvent was approximated by scaling electrostatic interactions with a simple distance-dependent dielectric function with $\varepsilon = 4r$. Non-bonded interactions were truncated after 18 Å with a switching function applied from 16 to 18 Å. NMA requires that the input structure corresponds to a local minimum in the potential energy function. Each structure was therefore extensively minimized using the adopted-basis Newton-Raphson algorithm until the energy changed less than 10^{-5} kcal/mol between subsequent steps. Typically, this was achieved in 10,000 to 40,000 minimization steps. At that time the remaining root mean square energy gradient was between 0.006 and 0.017 kcal/mol/Å. For each structure, the 5,000 lowest-frequency modes were extracted. These modes include six translation and rotational modes as well as three additional zero-frequency modes for each of 10 Zn^{2+} and Mg^{2+} ions[21]. All of the remaining 4,964 modes had positive frequencies and were used in the subsequent mode analysis.

In order to visualize and analyze the lowest-frequency modes, mode vectors scaled by a constant factor of +/−500 were added to the minimized structures.

Analysis

Root mean square fluctuations around the minimized structure can be calculated from the normal mode spectrum according to:

$$\sigma_i^2 = k_B T \sum_{n=1}^{N_{\max}} \frac{\mathbf{v}_{in}^2}{\omega_n^2} \quad (2)$$

where σ_i is the root mean square fluctuation for atom i, $\mathbf{v}_{in}$ is the mass-weighted eigenvector component for atom i and mode n as reported by CHARMM, and ω_n is the angular frequency of mode n, k_B is Boltzmann's constant, and T is the temperature. It should be noted that although BNM frequencies are not equivalent to exact frequencies from full NMA, the exact frequencies can be recovered by simple scaling as described elsewhere[36]. Here the scaled BNM frequencies were used in Eq. 2. The summation runs over the N_{max} lowest-frequency modes because the largest contributions to σ_i come from the lowest-frequency modes and higher-frequency modes contribute only very little.

Mode overlap between modes m and n, o_{mn}, was calculated from the eigenvectors $\mathbf{v}_n$ according to:

$$o_{mn} = \frac{|\mathbf{v}_m \cdot \mathbf{v}_n|}{|\mathbf{v}_m|\,|\mathbf{v}_n|} \quad (3)$$

Only C_α atoms were used for calculating the mode overlap. Only protein residues were used in mode comparisons. Mode overlap values may range from 0 (no overlap) to 1 (complete overlap), with values above 0.5 considered to be representative of significant overlap.

Results

RNA polymerase flexibility

The collective set of all normal modes describes enzyme flexibility as a function of residue in terms of root mean square fluctuations (RMSF). RMSF values are directly related to crystallographic B-factors. RMSF values were calculated according to Eq. 2 from the 5,000 lowest-frequency normal modes in order to analyze overall enzyme flexibility. The resulting RMSF profiles are shown in Fig. 2. The normal mode derived RMSF values are compared to RMSF values calculated from experimental B-factors as given in the PDB files of the crystal structures. It is immediately apparent that the experimental RMSF values from B-factors are much larger in magnitude and vary less as a function of residue than the calculated RMSF values. This is assumed to be largely a consequence of the low resolution of the crystal structures (3.5–4.0 Å). The calculated RMSF profiles therefore provide a more detailed view of RNAPII's flexibility than can currently be determined from experiments. We also calculated an RMSF profile from NMA calculations of bacterial RNA polymerase (data not shown), which agrees closely with previously published RMSF profiles for bacterial RNA polymerase[21]. Although the structures are different, structurally comparable parts are readily aligned between the two enzymes and show similar degrees of flexibility. The flexibility of RNAPII is illustrated further in Fig. 1B in which the residue-level flexibility is projected onto the crystal structure. As noted previously for bacterial RNA polymerase[7,21], RNAPII also has a rigid core that is surrounded by flexible domains. In particular the jaw and clamp domains exhibit significant flexibility.

In order to address the role of RNAPII dynamics during translocation, the change of flexibility as a result of trigger loop closing and NTP binding was examined by comparing RMSF profiles between the RNAPII-open (post-translocated, no NTP bound), RNAPII-

closed (NTP bound), and RNAPII-ntp states. According to Figs. 1 and 2 there are many regions where residue mobility appears to be affected by trigger helix formation. Most prominent is a rigidification of the clamp domain that holds the downstream DNA and to a lesser extent of the opposing jaw domain as a result of trigger helix formation. Less surprising is that the trigger loop, the proximal bridge helix, and neighboring structural parts also become less mobile when the trigger loop converts to a helical form. The change in overall flexibility as a result of binding NTP to the open trigger loop structure is less pronounced, but also involves a rigidification of parts of the clamp and jaw domains as a result of NTP binding (see Fig. 1D).

The reduced flexibility of the clamp domain upon trigger loop closing or NTP binding to the active site is assumed to translate into reduced mobility of the downstream DNA thereby effectively inhibiting translocation. An inhibition of translocation as a result of NTP binding would be expected based on functional and structural considerations, but the results presented here offer the additional insight that trigger loop opening may be required for translocation to proceed.

Enzyme motions described by individual modes

An analysis of individual low-frequency modes promises direct insight into the enzyme motions associated with specific biological mechanisms. The clamp opening/closing mode[21–23] in RNAP has been described previously, but other modes of RNA polymerase have not yet been characterized. Here, the 20 lowest-frequency modes of RNAPII were analyzed in detail.

One issue with the interpretation of individual modes from NMA is the possibility for mode mixing and more generally a lack of robustness as formalized by Thirumalai et al.[22]. A lack of robustness is manifested in sensitivity of a given mode to structure, sequence, or interaction potential perturbations and generally means that the motion described by such a mode is not conserved and thereby not necessarily meaningful. However, Thirumalai et al. found that modes lacking robustness may form small clusters in which the combined motions are conserved[40].

In order to support the following analysis of individual modes of RNAPII, we first analyzed the robustness of the lowest-frequency modes by comparing the four sets of modes for the four different states of RNAPII considered here (see Table 1). The modes are compared by calculating overlap values according to Eq. 3 for which a high overlap value close to 1 indicates mode conservation between two different structures. The mode overlap values for the 20 lowest-frequency modes between all pairs of states are given in Fig. 3. It is found that the first five modes are highly conserved across all states, while significant overlap between open and closed trigger loop states extends approximately to mode 10 and most of the 20 lowest-frequency modes are conserved within open trigger loop states. For the most part, the ordering of the modes is also maintained and the mode frequencies are preserved to within 0.1–0.2 cm^{-1}.

In order to visualize mode conservation further, a network diagram was constructed form the data in Fig. 3. In this network, the 10 lowest-frequency modes for each of the four states form nodes that are connected by edges only if significant overlap exists. It should be noted that there are no edges between different modes of the same state because normal modes are constructed to form an orthogonal basis set. The resulting diagram shown in Fig. 4 indicates distinct clusters for the first six modes with one mode from each state with no or only weak connections to other clusters. Different mode numbers within the same cluster indicate reordering of modes in terms of frequency which may result from minor structural perturbations and is not considered to be significant for the purposes of this study. Such

clustering indicates that these modes are robust with respect to the structural perturbations in the different RNAPII states considered here. Modes 7 and 8 (from RNAPII-open) form a two-mode cluster that indicates that the combined motion resulting from those two modes appears to be conserved. Such a combined motion may be a complex motion with modes 7 and 8 forming the basis vectors or a sequential motion that involves first one mode and then the other mode which cannot be distinguished from normal mode analysis. Modes 9 and 10 (from RNAPII-open) forms a similarly conserved cluster, but with three RNAPII-pre modes and lower degrees of overlap between modes. Overall these results suggest that the subspace spanned by the 10 lowest-frequency modes is quite robust in line with expectations from previous studies[41,42]. Higher modes form essentially one large cluster (data not shown) indicating extensive mode mixing and low robustness above mode 10. Based on these results we focus in the following discussion on the lowest 10 modes because they appear to be most robust and therefore most likely to describe functionally-relevant motions.

The motions resulting from the 10 lowest-frequency modes of RNAPII-open are depicted in Fig. 5. Movies of those motions are given as supplementary material. All of the modes involve global motions that couple multiple domains of RNAPII. Mode 1 most closely resembles the well-know clamp/jaw opening motion that is conserved among polymerases[21–23], but other modes also involve significant motion of the jaw and/or clamp domains. In particular, mode 2 also describes clamp/jaw opening albeit with more of a twisting motion. Modes 3, 4, and 5 couple different parts of the clamp and jaw domains near the tip to rpb8, rpb11, and/or rpb3 at the opposite end of RNAPII. Mode 6 again involves largely the clamp and jaw domains. Modes 7 and 8 involve motions of rpb1 and rpb5 near the downstream DNA and rpb2 near the DNA:RNA hybrid, especially in mode 8. Modes 9 and 10 again couple clamp/jaw motions to rpb11 and rpb8, but in contrast to modes 3, 4, and 5 central parts of the enzyme are involved to a greater extent, in particular rpb6.

Nucleic acid motion during individual modes

In order to focus on translocation we now consider motions of the nucleic acid during the 10 lowest-frequency modes (Fig. 6). It is immediately apparent that all of the low-frequency modes result in significant motion of the nucleic acid complex. In particular, the downstream DNA moves significantly in all modes except for mode 8. This is not unexpected because the downstream DNA interacts closely with the clamp domain, which is mobile in many of the modes as described above. The downstream DNA moves in different directions in different modes. Only in mode 2 and to a lesser extent in modes 6 and 7 does the DNA move parallel to the downstream helical axis as would be expected during translocation. In modes 5, 9, and 10, the downstream DNA motion is at an angle to the helical axis. In the remaining modes the downstream DNA moves nearly perpendicular to the helical axis. The downstream DNA translocation motion is quantified further by calculating the distance between the N5/T10 base pair at the center of downstream DNA helix and the position of the C1′ atom in the active site template base T18 from the minimized structure of RNAPII-open (see Table 2). It is found that the effective translocation towards the active site is largest in mode 7, but it is also significant in modes 2, 5, and 9. While essentially all modes involve some motion in the downstream DNA helix, the single-stranded template strand and DNA:RNA hybrid move significantly only in modes 7 and 8. In mode 7 the single-stranded DNA and the first few base pairs of the DNA:RNA hybrid move along the helical axis of the DNA:RNA hybrid. In mode 8, the upstream part of the DNA:RNA hybrid moves significantly including an apparent strand separation motion where the template strand is pulled away from the RNA. As shown in Fig. 5, this motion is coupled to a large motion of a part of rpb2 near the end of the DNA:RNA hybrid away from the nucleic acid that appears to pull the template strand along. Based on these findings it is hypothesized that the combination of modes 7 and 8 describes the dynamics associated with

nucleic acid translocation. In addition, mode 2 may describe independent translocation of the downstream DNA helix. A motion of the nucleic acid complex similar to mode 2 was also observed in molecular dynamics simulations of RNAPII, although the simulations did not show the extensive clamp/jaw motions indicated by mode 2 (M. Feig and Z. Burton: unpublished data).

Modes 7 and 8 were further compared between RNAPII-open, RNAPII-pre, RNAPII-ntp, and RNAPII-closed as shown in Fig. 7. According to the mode overlap analysis described above modes 7 and 8 form a cluster suggesting that the combined motions from both modes should be considered. In RNAPII-open and RNAPII-pre, the states in which forward or backward translocation is expected to be possible, the combination of modes 7 and 8 would lead to translocation of the entire nucleic acid complex including separation of the upstream end of the DNA:RNA hybrid.

In RNAPII-ntp, mode 7 exhibits upstream DNA:RNA hybrid translocation along with significant motion of the downstream DNA at an angle with respect to the helical axis and combined with a small amount of translocation of the DNA:RNA hybrid near the active site. At the same time, mode 8 of RNAPII-ntp closely resembles mode 7 of RNAPII-open/RNAPII-pre with the motion of the downstream DNA directed more along its helical axis and more significant motion of the template strand near the active site. However, although difficult to see in the figure, the forward motion of the template strand is coupled to backward motion of the DNA:RNA hybrid. Neither one of the modes 7 or 8 of RNAPII-ntp appears to be sufficient to translocate the nucleic acid complex. However, a combined motion according to modes 7 and 8 would result in a very large motion of the downstream DNA, mostly at an angle to its helical axis, relative to the motion of the DNA:RNA hybrid that would be diminished by the backward motion in mode 8. Therefore, it appears as a result of the mode analysis that translocation is effectively frustrated when NTPs are bound in the active site. This is consistent with the expectation that translocation should not occur until an NTP has been incorporated and the pre-translocated state has been reached.

Modes 7 and 8 of RNAPII-closed are more similar to RNAPII-open and RNAPII-pre, but with two important differences: The mode vectors of mode 8 at the end of the DNA:RNA hybrid indicate possible translocation but not strand separation. Furthermore, the combination of modes 7 and 8 would result in significant motion of the downstream DNA relative to DNA:RNA translocation (or diminished DNA:RNA translocation relative to the downstream DNA motion). As in the RNAPII-ntp case, these results are therefore also interpreted to suggest that productive translocation is inhibited with a closed trigger loop.

Bridge helix bending

Previous studies have indicated that bridge helix bending may play a key role in the functional cycle of RNA polymerase[9]. Therefore, the degree to which bridge helix bending changes in different modes was investigated here as well. The bending angle of the bridge helix was calculated as the angle between the vector from rpb1 811 to 825 and the vector from rpb1 830 to 843. With this definition, a perfectly straight helix would correspond to an angle of 180°. Fig. 8 shows the change in bridge helix bending from the initial structures based on the scaled mode vector displacements (see methods). The initial bending values are given in the caption of Fig. 8. The actual magnitude of the change in bending angles is arbitrary because it depends on the arbitrary scaling of the mode vectors. However, the relative differences between different modes are considered to be meaningful. The largest change is observed in mode 7 which is closely associated with translocation. Significant changes in bridge helix bending are also seen in modes 3, 8, 9, and 10. These results indicate that the bridge helix exhibits significant bending flexibility and provide further evidence that bridge helix bending is intimately coupled to translocation.

An interesting finding is the apparent asymmetry of bridge helix bending in modes 7 and 8 of RNAPII-open and RNAPII-pre, both of which move the nucleic acid complex in a similar manner (see Fig. 7). For RNAPII-open, bridge helix bending is significantly larger in mode 7 than in mode 8, but for RNAPII-pre, bridge helix bending is larger in mode 8 compared to mode 7. This difference may reflect different motions during forward translocation of RNAPII-pre and (presumed) backward translocation in RNAPII-open. One may speculate that forward translocation of the pre-translocated state involves modes 7 and 8 in coupled but sequential order with bridge helix bending playing a major role in forward translocation of the upstream DNA:RNA hybrid. In backward translocation of the post-translocated state mode 7 may initially straighten the bridge helix along with downstream translocation to facilitate backtracking of the DNA:RNA hybrid through mode 8 in the coupled second step.

Discussion and Conclusion

RNA polymerase is of fundamental importance for the transcription process, yet despite extensive information from crystallographic structures, many aspects of its functional mechanism remain elusive. Here, we present a first analysis of dynamic features in eukaryotic RNA polymerase II based on computational normal mode analysis. The main focus of this analysis is on the translocation mechanism and in particular on how global changes of the enzyme structure may facilitate translocation.

Several low-frequency modes were identified in which the downstream DNA moves along its helical axis and the DNA:RNA hybrid is translocated in one mode (mode 8). It is hypothesized that a combination of modes 7 and 8 may describe translocation within the approximations of the NMA methodology used here. In addition, mode 2 suggests that the downstream DNA may also translocate independently from the DNA:RNA hybrid. These motions of the nucleic acid complex are coupled to motions of the clamp and jaw domains and parts of rpb2 near the end of the DNA:RNA hybrid. Furthermore, significant bridge helix bending is seen during the proposed translocation modes 7 and 8. This finding supports previous speculations that the bridge helix plays a key role during translocation[43]. A closer inspection of the modes suggests that complete translocation is inhibited in both the closed trigger helix state and the open trigger loop structures with NTP bound in the active site. A similar conclusion can also be found based on the observation of reduced clamp flexibility with a closed trigger loop or in the presence of NTP in the active site under the assumption that the clamp motion is necessary for translocation as indicated by the NMA modes.

The apparent coupling of clamp/jaw opening motions to nucleic acid translocation is interesting and has not been discussed previously to our knowledge. Such a coupling would explain experimental observations that link protein-protein interactions at the clamp to transcriptional efficiency. Hepatitis delta antigen, which binds to the human RNAPII clamp domain, accelerates elongation rates and compromises transcriptional fidelity[44]. Furthermore, proteins interacting with rpb5 at the side of the clamp domain have been found to negatively or positively affect transcription, such as RPB5-mediated protein in conjunction with TFIIF[45,46], hepatitis B virus X protein[46], TFIIB[47], and TIP120[48]. Additional experiments that could further validate the proposed role of clamp/jaw motion during translocation could involve FRET techniques in which suitable fluorescence reporters may be attached opposite from each other on the jaw and clamp domains. Because of the relatively large distance across the DNA binding cleft, such probes may be best positioned at the sides of the clamp/jaw domains. For example, probes could be attached at sites near residue 86 of rpb5 and residue 1219 or 1220 in rpb1. The distance between those sites varies considerably during the translocation-relevant mode 7. In the closed cleft conformation, a minimum distance of less than 12 Å between Cα atoms is reached. While FRET could confirm the large-scale domain motions predicted here, another possibility is chemical

cross-linking between the same residue pairs. Cross-linking studies could test 1) whether cross-linking is possible and 2) whether translocation is inhibited in the presence of such cross-links as would be predicted by the results from this study.

Full translocation of the nucleic acid complex must also involve downstream DNA unwinding, upstream DNA rewinding, RNA extrusion through the exit channel, and possible interactions of the single-stranded non-template strand. Because the present study relies on available crystal structures of RNAPII in which the nucleic acid part is comprised only of the downstream DNA and the DNA:RNA hybrid, none of these contributions to translocation with the exception of downstream DNA unwinding could be addressed here. There is no evidence that the single-stranded non-template strand or RNA exit significantly affect translocation, but recent experimental studies have suggested that upstream DNA rewinding affect elongation, presumably by enhancing the rate of translocation[49]. DNA unwinding is not observed in modes 2, 7, or 8, but some of the other modes, for example mode 4, move the downstream DNA in a shearing motion that visually resembles the beginning of DNA unwinding. However, because normal modes are strictly not able to describe true rotary motions, the significance of such motions is unclear. It does appear, though, that DNA unwinding may represent a separate step from linear nucleic acid translocation.

The NMA results presented here should be viewed primarily as a means to obtain a qualitative view of functionally-relevant motions in RNAPII that can be subjected to further theoretical and experimental exploration. More detailed insight and in particular thermodynamically meaningful results of specific aspects of RNAPII dynamics can be obtained from molecular dynamics simulations. Experimental tests of the proposed role of clamp/jaw motions are described above. Furthermore, mutational studies may target regions where a significant change in flexibility is observed as a result of trigger loop closing or NTP binding. For many of these sites, mutants have already been studied. They are summarized in Table 3. The mutations cover almost all of the regions in rpb1 and rpb2 where significant changes in flexibility are found. Additional sites of notable changes in flexibility that have not been examined in detail are parts of the jaw(2) domain, also called the protrusion domain (rpb2 residues 210–300), residues rpb2 863–870 near the RNA exit channel, rpb2 residues 732–734, and rpb2 residues 550–620. It is hypothesized that mutations in those regions may also compromise RNA polymerase function.

The present study provides new insight into the translocation mechanism of RNA polymerase. It is our hope that these results will encourage further experimental and computational studies that will ultimately lead to a complete understanding of the fundamental process of transcription.

Supplementary Material

Refer to Web version on PubMed Central for supplementary material.

Acknowledgments

We would like to thank Shayantani Mukherjee for discussions and critical comments. Sean Law is acknowledged for providing a script to generate illustrations of individual normal modes with PyMOL[50]. Financial support from NSF CAREER grant 0447799 (to MF) and NIH GM57461 (to ZFB) is acknowledged.

References

1. Lee TI, Young RA. Transcription of eukaryotic protein-coding genes. Annual Review of Genetics. 2000; 34:77–137.

2. Kornberg RD. Eukaryotic transcriptional control. Trends in Biochemical Sciences. 1999; 24(12):M46–M49.

3. Borukhov S, Nudler E. RNA polymerase: the vehicle of transcription. Trends in Microbiology. 2008; 16(3):126–134. [PubMed: 18280161]

4. Cramer P, Armache KJ, Baumli S, Benkert S, Brueckner F, Buchen C, Damsma GE, Dengl S, Geiger SR, Jasiak AJ, Jawhari A, Jennebach S, Kamenski T, Kettenberger H, Kuhn CD, Lehmann E, Leike K, Sydow JF, Vannini A. Structure of Eukaryotic RNA Polymerases. Annual Review of Biophysics. 2008; 37(1):337–352.

5. Hahn S. Structure and mechanism of the RNA polymerase II transcription machinery. Nat Struct Mol Biol. 2004; 11:394. [PubMed: 15114340]

6. Cramer P. RNA polymerase II structure: from core to functional complexes. Current Opinion in Genetics & Development. 2004; 14(2):218–226. [PubMed: 15196470]

7. Darst SA, Opalka N, Chacon P, Polyakov A, Richter C, Zhang GY, Wriggers W. Conformational flexibility of bacterial RNA polymerase. Proc Natl Acad Sci USA. 2002; 99(7):4296–4301. [PubMed: 11904365]

8. Coban O, Lamb DC, Zaychikov E, Heumann H, Nienhaus GU. Conformational heterogeneity in RNA polymerase observed by single-pair FRET microscopy. Biophys J. 2006; 90(12):4605–4617. [PubMed: 16581837]

9. Bar-Nahum G, Epshtein V, Ruckenstein AE, Rafikov R, Mustaev A, Nudler E. A ratchet mechanism of transcription elongation and its control. Cell. 2005; 120(2):183–193. [PubMed: 15680325]

10. Vassylyev DG, Artsimovitch I. Tracking RNA polymerase, one step at a time. Cell. 2005; 123(6): 977–979. [PubMed: 16360025]

11. Guo Q, Sousa R. Translocation by T7 RNA polymerase: A sensitively poised Brownian ratchet. J Mol Biol. 2006; 358:241–254. [PubMed: 16516229]

12. Thomen P, Lopez PJ, Heslot F. Unravelling the mechanism of RNA-polymerase forward motion by using mechanical force. Phys Rev Lett. 2005; 94(12)

13. Abbondanzieri EA, Greenleaf WJ, Shaevitz JW, Landick R, Block SM. Direct observation of base-pair stepping by RNA polymerase. Nature. 2005; 438(7067):460–465. [PubMed: 16284617]

14. Bai L, Santangelo TJ, Wang MD. Single-molecule analysis of RNA polymerase transcription. Annu Rev Biophys Biomol Struct. 2006; 35:343–360. [PubMed: 16689640]

15. Burton ZF, Feig M, Gong XQ, Zhang CF, Nedialkov YA, Xiong YL. NTP-driven translocation and regulation of downstream template opening by multi-subunit RNA polymerases. Biochemistry and Cell Biology-Biochimie Et Biologie Cellulaire. 2005; 83(4):486–496. [PubMed: 16094452]

16. Zhou Y, Navaroli DM, Enuameh MS, Martin CT. Dissociation of halted T7 RNA polymerase elongation complexes proceeds via a forward-translocation mechanism. Proc Natl Acad Sci USA. 2007; 104(25):10352–10357. [PubMed: 17553968]

17. Yin YW, Steitz TA. The structural mechanism of translocation and helicase activity in T7 RNA polymerase. Cell. 2004; 116(3):393–404. [PubMed: 15016374]

18. Wang D, Bushnell DA, Westover KD, Kaplan CD, Kornberg RD. Structural basis of transcription: Role of the trigger loop in substrate specificity and catalysis. Cell. 2006; 127(5):941–954. [PubMed: 17129781]

19. Vassylyev DG, Vassylyeva MN, Zhang J, Palangat M, Artsimovitch I, Landick R. Structural basis for substrate loading in bacterial RNA polymerase. Nature. 2007; 448:163. [PubMed: 17581591]

20. Woo HJ, Liu Y, Sousa R. Molecular dynamics studies of the energetics of translocation in model T7 RNA polymerase elongation complexes. Proteins. 2008; 73(4):1021–1036. [PubMed: 18536012]

21. Van Wynsberghe A, Li GH, Cui Q. Normal-mode analysis suggests protein flexibility modulation throughout RNA polymerase's functional cycle. Biochemistry. 2004; 43(41):13083–13096. [PubMed: 15476402]

22. Zheng WJ, Brooks BR, Doniach S, Thirumalai D. Network of dynamically important residues in the open/closed transition in polymerases is strongly conserved. Structure. 2005; 13(4):565–577. [PubMed: 15837195]

23. Delarue M, Sanejouand YH. Simplified normal mode analysis of conformational transitions in DNA-dependent polymerases: the Elastic Network Model. J Mol Biol. 2002; 320(5):1011–1024. [PubMed: 12126621]
24. Van Wynsberghe AW, Cui Q. Comparison of mode analyses at different resolutions applied to nucleic acid systems. Biophys J. 2005; 89(5):2939–2949. [PubMed: 16100266]
25. Fiser A, Do RKG, Sali A. Modeling of Loops in Protein Structures. Protein Sci. 2000; 9:1753–1773. [PubMed: 11045621]
26. Sali A, Blundell TL. Comparative Protein Modelling by Satisfaction of Spatial Restraints. J Mol Biol. 1993; 234:779–815. [PubMed: 8254673]
27. Brooks BR, Brooks CL III, Mackerell AD Jr, Nilsson L, Petrella RJ, Roux B, Won Y, Archontis G, Bartels C, Boresch S, Caflisch A, Caves L, Cui Q, Dinner AR, Feig M, Fischer S, Gao J, Hodoscek M, Im W, Kuczera K, Lazaridis T, Ma J, Ovchinnikov V, Paci E, Pastor RW, Post CB, Pu JZ, Schaefer M, Tidor B, Venable RM, Woodcock HL, Wu X, Yang W, York DM, Karplus M. CHARMM: The biomolecular simulation program. J Comput Chem. 2009; 30(10):1545–1614. [PubMed: 19444816]
28. MacKerell AD Jr, Bashford D, Bellott M, Dunbrack JD, Evanseck MJ, Field MJ, Fischer S, Gao J, Guo H, Ha S, Joseph-McCarthy D, Kuchnir L, Kuczera K, Lau FTK, Mattos C, Michnick S, Ngo T, Nguyen DT, Prodhom B, Reiher WE, Roux B, Schlenkrich M, Smith JC, Stote R, Straub J, Watanabe M, Wiorkiewicz-Kuczera J, Yin D, Karplus M. All-Atom Empirical Potential for Molecular Modeling and Dynamics Studies of Proteins. J Phys Chem B. 1998; 102:3586–3616.
29. Brooks BR, Janezic D, Karplus M. Harmonic-Analysis of Large Systems. 1. Methodology. J Comput Chem. 1995; 16(12):1522–1542.
30. Tama F, Valle M, Frank J, Brooks CL. Dynamic reorganization of the functionally active ribosome explored by normal mode analysis and cryo-electron microscopy. Proc Natl Acad Sci USA. 2003; 100(16):9319–9323. [PubMed: 12878726]
31. Tama F, Feig M, Liu J, Brooks CL, Taylor KA. The requirement for mechanical coupling between head and S2 domains in smooth muscle myosin ATPase regulation and its implications for dimeric motor function. J Mol Biol. 2005; 345(4):837–854. [PubMed: 15588830]
32. Zheng W, Brooks BR, Thirumalai D. Allosteric transitions in the chaperonin GroEL are captured by a dominant normal mode that is most robust to sequence variations. Biophys J. 2007; 93(7): 2289–2299. [PubMed: 17557788]
33. Brooks B, Karplus M. Normal-Modes for Specific Motions of Macromolecules – Application to the Hinge-Bending Mode of Lysozyme. Proc Natl Acad Sci USA. 1985; 82(15):4995–4999. [PubMed: 3860838]
34. Doruker P, Jernigan RL, Bahar I. Dynamics of large proteins through hierarchical levels of coarse-grained structures. J Comput Chem. 2002; 23(1):119–127. [PubMed: 11913377]
35. Tama F, Gadea FX, Marques O, Sanejouand YH. Building-block approach for determining low-frequency normal modes of macromolecules. Proteins. 2000; 41(1):1–7. [PubMed: 10944387]
36. Li GH, Cui Q. A coarse-grained normal mode approach for macromolecules: An efficient implementation and application to Ca2+-ATPase. Biophys J. 2002; 83(5):2457–2474. [PubMed: 12414680]
37. Brooks BR, Bruccoleri RE, Olafson BD, States DJ, Swaminathan S, Karplus M. CHARMM: A Program for Macromolecular Energy, Minimization, and Dynamics Calculations. J Comput Chem. 1983; 4:187–217.
38. Foloppe N, MacKerell AD Jr. All-Atom Empirical Force Field for Nucleic Acids: I. Parameter Optimization Based on Small Molecule and Condensed Phase Macromolecular Target Data. J Comput Chem. 2000; 21:86–104.
39. MacKerell AD Jr, Feig M, Brooks CL III. Extending the treatment of backbone energetics in protein force fields: Limitations of gas-phase quantum mechanics in reproducing protein conformational distributions in molecular dynamics simulations. J Comput Chem. 2004; 25:1400–1415. [PubMed: 15185334]
40. Zheng W, Thirumalai D. Coupling between Normal Modes Drives Protein Conformational Dynamics: Illustrations Using Allosteric Transitions in Myosin II. Biophys J. 2009; 96(6):2128–2137. [PubMed: 19289039]

41. Yang L-W, Eyal E, Bahar I, Kitao A. Principal component analysis of native ensembles of biomolecular structures (PCA_NEST): insights into functional dynamics. Bioinformatics. 2009; 25(5):606–614. [PubMed: 19147661]
42. Nicolay S, Sanejouand YH. Functional Modes of Proteins Are among the Most Robust. Phys Rev Lett. 2006; 96(7):078104. [PubMed: 16606146]
43. Kaplan C, Kornberg R. A bridge to transcription by RNA polymerase. Journal of Biology. 2008; 7(10):39. [PubMed: 19090964]
44. Yamaguchi Y, Mura T, Chanarat S, Okamoto S, Handa H. Hepatitis delta antigen binds to the clamp of RNA polymerase II and affects transcriptional fidelity. Genes Cells. 2007; 12(7):863–875. [PubMed: 17584298]
45. Wei WX, Gu JX, Zhu CQ, Sun FY, Dorjsuren D, Lin Y, Murakami S. Interaction with general transcription factor IIF (TFIIF) is required for the suppression of activated transcription by RPB5-mediating protein. Cell Res. 2003; 13(2):111–120. [PubMed: 12737519]
46. Le TTT, Zhang SJ, Hayashi N, Yasukawa M, Delgermaa L, Murakami S. Mutational analysis of human RNA polymerase II subunit 5 (RPB5): The residues critical for interactions with TFIIF subunit RAP30 and hepatitis B virus X protein. J Biochem. 2005; 138(3):215–224. [PubMed: 16169872]
47. Todone F, Weinzierl ROJ, Brick P, Onesti S. Crystal structure of RPB5, a universal eukaryotic RNA polymerase subunit and transcription factor interaction target. Proc Natl Acad Sci USA. 2000; 97(12):6306–6310. [PubMed: 10841537]
48. Makino Y, Yogosawa S, Kayukawa K, Coin F, Egly JM, Wang ZX, Roeder RG, Yamamoto K, Muramatsu M, Tamura TA. TATA-binding protein-interacting protein 120, TIP120, stimulates three classes of eukaryotic transcription via a unique mechanism. Molecular and Cellular Biology. 1999; 19(12):7951–7960. [PubMed: 10567521]
49. Naji S, Bertero MG, Spitalny P, Cramer P, Thomm M. Structure-function analysis of the RNA polymerase cleft loops elucidates initial transcription, DNA unwinding and RNA displacement. Nucleic Acids Res. 2008; 36(2):676–687. [PubMed: 18073196]
50. DeLano, WL. The PyMOL Molecular Graphics System. DeLano Scientific; San Carlos, CA: 2002.
51. Donaldson IM, Friesen JD. Zinc stoichiometry of yeast RNA polymerase II and characterization of mutations in the zinc-binding domain of the largest subunit. J Biol Chem. 2000; 275(18):13780–13788. [PubMed: 10788499]
52. Archambault J, Drebot MA, Stone JC, Friesen JD. Isolation and Phenotypic Analysis of Conditional-Lethal, Linker-Insertion Mutations in the Gene Encoding the Largest Subunit of Rna Polymerase-Ii in Saccharomyces-Cerevisiae. Molecular & General Genetics. 1992; 232(3):408–414. [PubMed: 1588909]
53. Malagon F, Kireeva ML, Shafer BK, Lubkowska L, Kashlev M, Strathern JN. Mutations in the Saccharomyces cerevisiae RPB1 gene conferring hypersensitivity to 6-azauracil. Genetics. 2006; 172(4):2201–2209. [PubMed: 16510790]
54. Scafe C, Martin C, Nonet M, Podos S, Okamura S, Young RA. Conditional Mutations Occur Predominantly in Highly Conserved Residues of Rna Polymerase-Ii Subunits. Molecular and Cellular Biology. 1990; 10(3):1270–1275. [PubMed: 2406567]
55. Trinh V, Langelier MF, Archambault J, Coulombe B. Structural perspective on mutations affecting the function of multisubunit RNA polymerases. Microbiology and Molecular Biology Reviews. 2006; 70(1):12–+. [PubMed: 16524917]
56. Wang D, Bushnell D, Westover K, Kaplan C, Kornberg R. Structural basis of transcription: role of the trigger loop in substrate specificity and catalysis. Cell. 2006; 127:941–954. [PubMed: 17129781]
57. Vassylyev DG, Vassylyeva MN, Perederina A, Tahirov TH, Artsimovitch I. Structural basis for transcription elongation by bacterial RNA polymerase. Nature. 2007; 448:157. [PubMed: 17581590]
58. Archambault J, Jansma DB, Kawasoe JH, Arndt KT, Greenblatt J, Friesen JD. Stimulation of transcription by mutations affecting conserved regions of RNA polymerase II. Journal of Bacteriology. 1998; 180(10):2590–2598. [PubMed: 9573141]

59. Toulokhonov I, Zhang JW, Palangat M, Landick R. A central role of the RNA polymerase trigger loop in active-site rearrangement during transcriptional pausing. Mol Cell. 2007; 27(3):406–419. [PubMed: 17679091]

60. Kaplan CD, Larsson KM, Kornberg RD. The RNA polymerase II trigger loop functions in substrate selection and is directly targeted by alpha-amanitin. Mol Cell. 2008; 30(5):547–556. [PubMed: 18538653]

61. Archambault J, Lacroute F, Ruet A, Friesen JD. Genetic Interaction between Transcription Elongation-Factor Tfiis and Rna Polymerase-Ii. Molecular and Cellular Biology. 1992; 12(9): 4142–4152. [PubMed: 1508210]

62. Humphrey W, Dalke A, Schulten K. VMD: Visual molecular dynamics. J Mol Graph. 1996; 14(1): 33–&. [PubMed: 8744570]

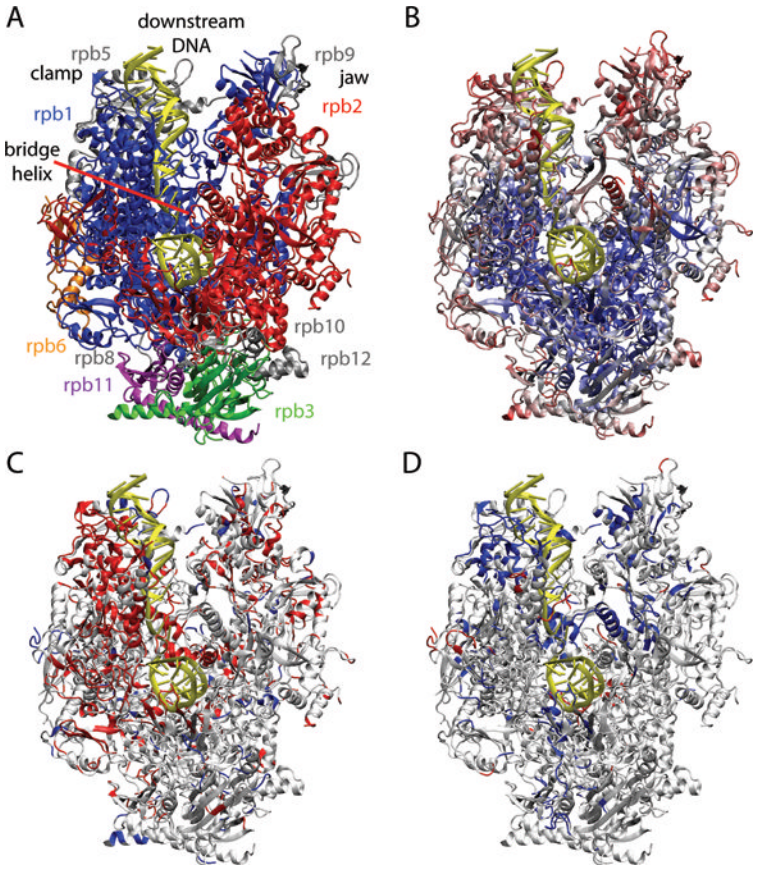

Figure 1.

S. cerevisiae RNA polymerase II structure (PDB: 2E2J[18]) (A); normal mode-derived RMSFs for C_α atoms projected onto the minimized crystal structure of RNAPII (B) where rigid regions (<0.5 Å^2) are indicated in blue, flexible regions (>0.7 Å^2) in red, and regions of average flexibility (around 0.6 Å^2) are shown in white; change in flexibility of normal mode-derived RMSFs between open and closed trigger loop structures of RNAPII (C) and between open trigger loop structures with and without a nucleotide in the active site (D). A relative increase (decrease) in flexibility by more than 10% from the closed to the open trigger loop structure is indicated in red (blue). A relative increase (decrease) by more than 7% from the nucleotide-free open trigger loop structure to the nucleotide-bound structure is indicated in red (blue). All figures were created with VMD[62].

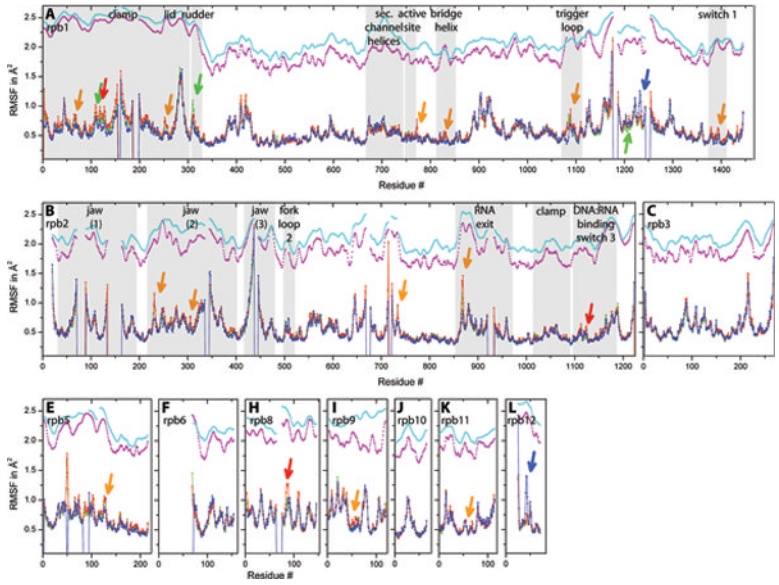

Figure 2.

Root mean square fluctuations (RMSF) for C_α atoms as a function of residue for RNAPII. Normal mode-derived RMSF values are shown as a solid line in red (RNAPII-open), green (RNAPII-ntp), and blue (RNAPII-closed). RMSF values calculated from experimental B-factors are shown as a dotted line in cyan (2E2H, closed trigger loop) and magenta (2E2J, open trigger loop). Residues profiles are shown separately for chains A (rpb1), B (rpb2), C (rpb3), E (rpb5), F (rpb6), H (rpb8), I (rpb9), J (rpb10), K (rpb11), L (rpb12). Arrows indicate significant differences in flexibility based on percentage change from the least flexible structure. Arrow colors indicate deviations in RNAPII-open (red), RNAPII-ntp (green), RNAPII-closed (blue), and both RNAPII-open and RNAPII-ntp (orange).

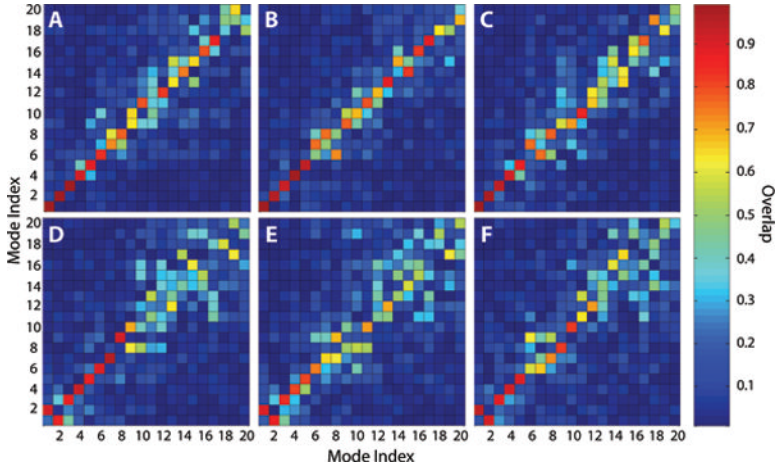

Figure 3.

Mode overlap between the 20 lowest-frequency modes for different states of RNAPII according to Eq. 3. **A**: RNAPII-ntp vs. RNAPII-open; **B**: RNAPII-pre vs. RNAPII-open; **C**: RNAPII-pre vs. RNAPII-ntp; **D**: RNAPII-closed vs. RNAPII-open; **E**: RNAPII-closed vs. RNAPII-ntp; **F**: RNAPII-closed vs. RNAPII-pre. The degree of overlap (ranging from 0 to 1) is indicated in color according to the bar on the right.

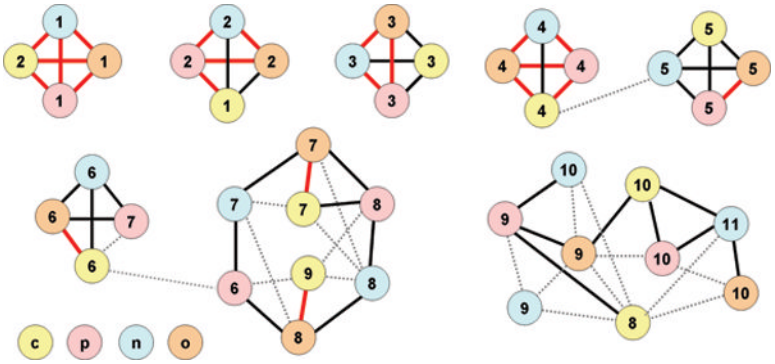

Figure 4.

Mode correspondence network in RNAPII based on the mode overlap data from Fig. 3 for the ten lowest-frequency modes. Each mode is represented as a number enclosed in a circle. Circles are colored according to the RNAPII state (*tan*: RNAPII-open; *pink*: RNAPII-pre; *cyan*: RNAPII-ntp; *yellow*: RNAPII-closed). Modes are connected with thick red lines if strongly correlated (overlap value > 0.9), with solid black lines if moderately correlated (overlap values of 0.7–0.9), and with dashed grey lines if weakly correlated (overlap values of 0.5–0.7).

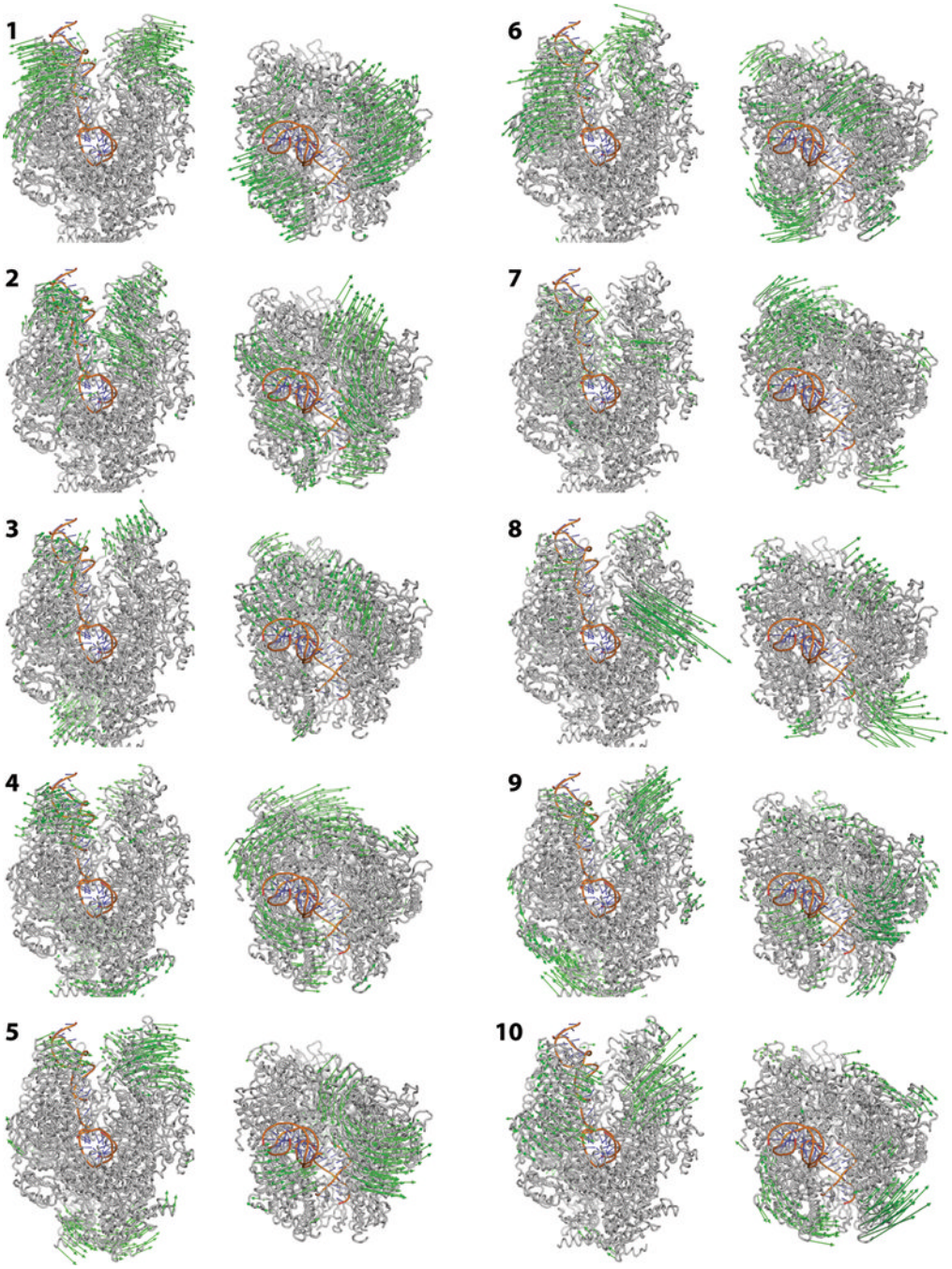

Figure 5.
RNA polymerase motions during ten lowest-frequency modes of RNAPII-open indicated as arrows. The illustrations were generated using PyMol[50]. Movies of these motions are available in the supplementary material.

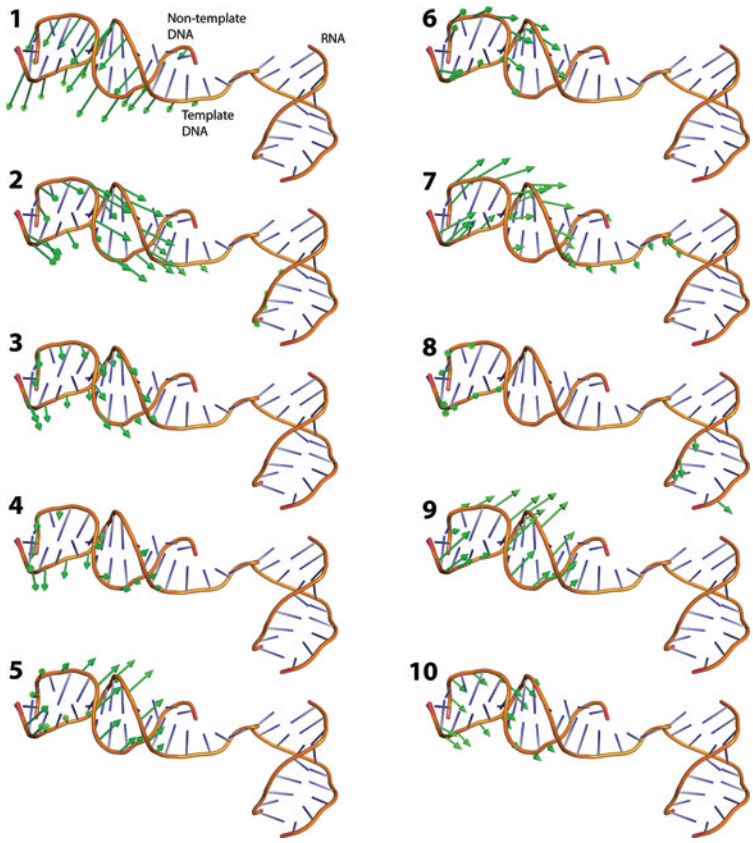

Figure 6.

Nucleic acid motions projected onto phosphorous atoms during the ten lowest-frequency modes of RNAPII-open indicated as arrows. The arrow lengths are equal to five times the actual displacement seen in the modes, displacements of less than 1 Å are not shown. The illustrations were generated using PyMOL[50].

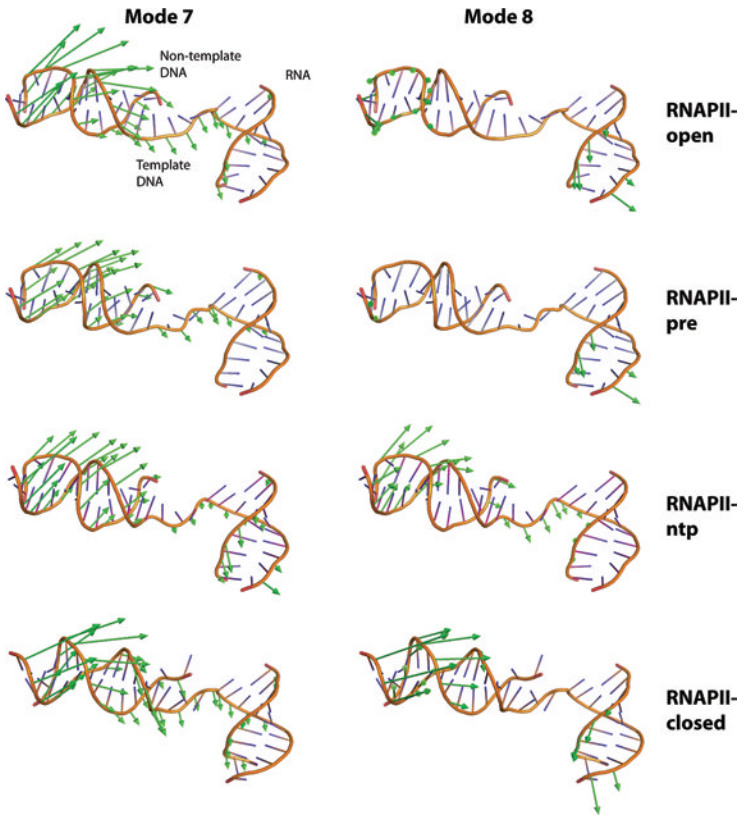

Figure 7.

Nucleic acid motions of modes 7 and 8 from RNAPII-open, RNAPII-pre, RNAPII-ntp, and RNAPII-closed as in Figure 7 but with arrow lengths equal to ten times the actual displacement seen in the modes and all displacements of more than 0.5 Å are shown to magnify motions proposed to be involved in translocation. The illustrations were generated using PyMOL[50].

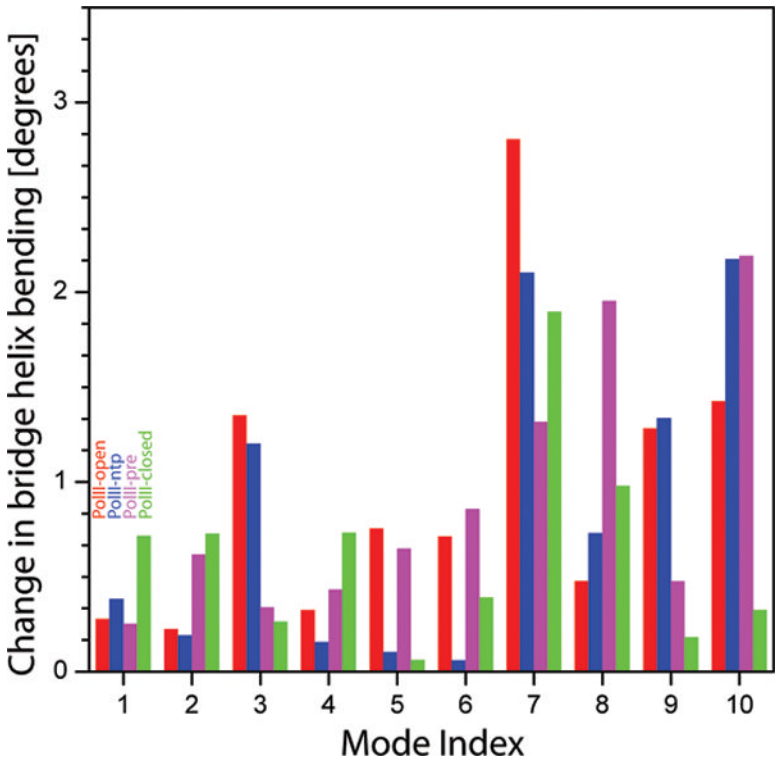

Figure 8.

Relative change in bridge helix bending for lowest-frequency modes in RNAPII. The RNAPII modes are numbered and ordered according to the RNAPII-open modes (red) with corresponding RNAPII-ntp (blue), RNAPII-pre (magenta), and RNAPII-closed (green) modes according to Fig. 4. Thus, the green bar for RNAPII mode 1, e.g., corresponds to mode 2 of RNAPII-closed and not to mode 1 of RNAPII-closed. The initial bridge helix bending angles of the minimized crystal structures were: 157.8° for RNAPII-open, 155.2° for RNAPII-ntp, 158.4° for RNAPII-pre, and 151.7° for RNAPII-closed.

Table 1

Overview of studied RNA polymerase structures from *S. cerevisiae*.

Name	PDB ID	Active site NTP	Trigger loop	C_α RMSD after min. [Å]
RNAPII-open	2E2J[18]	none	open	2.47
RNAPII-ntp	2E2J	GTP	open	2.01
RNAPII-pre	2E2J	Guanine	open	2.29
RNAPII-closed	2E2H[18]	GTP	closed	2.53

Table 2

Decrease in distance of N5/T10 base pair from T18:C1′ atom in minimized structure of RNAPII-open during low-frequency modes of RNAPII-open

Mode	Δdistance (N5/T10 – T18:C1′) [Å]
1	0.62
2	0.85
3	0.17
4	0.16
5	0.75
6	0.42
7	1.17
8	0.01
9	1.14
10	0.62

Table 3

Examples of mutations in RNAPII (or homologs) at sites where enzyme flexibility is altered between open and closed trigger loop states by at least 10%. The change in RMSF is given relative to the open trigger loop structure. The observed effect of the mutation is abbreviated as follows: **ts**: temperature sensitive; –: lethal; **cs**: cold sensitive; **ino**: growth on inositol; **6-AU**: 6-azauracil sensitive; **sit**: suppressor of initiation defect; **ss**: start site selection

Subunit	Region	Mutation	Effect	ΔRMSF [%]
rpb1	clamp, RNA exit	G79D	ts[51]	−22
	clamp	Q124(ARAR)A	ts[52]	−31
	clamp, lid	D260N	6-AU[53]	−16
	clamp, lid	Δ248–261	–[49]	up to −45
	rudder	R320C	6-AU[53]	−22
	rudder	Δ303–325	–[49]	up to −53
	surface feature	R412H	cs, ts[54]	−13
	active site, Mg^{2+} bind.	many (470–488)[55]	varies	up to −26
	active site loop	others (750–753)[56,57]	varies	up to −31
	α-amanitin resistance	A759P	sit[58]	−10
	bridge helix	many (820–840)[43]	varies	up to −44
	trigger loop/helix	many (1070–1100)[59,60]	varies	up to −81
	cleft, TFIIS bind.	E1230K	ts[61], 6-AU[53]	+24
	cleft	L1236(TRARV)I	6-AU[61]	+24
rpb2	jaw(2)	C317Y	ss[55]	−11
	active site loop	A1016T[54], P1018S[54], R1020A[56]	varies	−15, −15, −18